Letters

Impact of Nonlinear AC Fault Arc Resistance on Commutation Failures in LCC-HVDC Systems

Chenguang Yan, *Senior Member, IEEE*, Hongxi Yang, *Graduate Student Member, IEEE*, Qinzhi Liu, Peng Zhang, *Graduate Student Member, IEEE*, and Baohui Zhang, *Fellow, IEEE*

***Abstract*—Commutation failures (CFs) in LCC-HVDC systems are typically caused by inverter-side ac line faults. Historically, since the fault arc resistance has been simplified to a fixed resistance in related studies, possible ac arc-induced bus voltage distortions have not been sufficiently studied. This letter investigates the impact of nonlinear ac fault arc resistance on CFs. Specifically, transient expressions for the commutation voltage–time area (VTA) under different fault types are derived. With a black-box arc model embedded in the analysis of the commutation process, periodic voltage distortions resulting from the nonlinear resistance of the fault arc appear in the faulty phase voltages. Notably, these spike-shaped voltage distortions result in a variation in the commutation VTA under single-line-to-ground faults close to the commutation bus. In addition, these impacts of the nonlinear arc resistance on CFs are verified through extensive simulations on the real-time digital simulator. This study reveals a hidden arc-induced feature that impacts CFs and bridges the gap between research on fault transients and the associated CFs.**

***Index Terms*—Commutation failure (CF), commutation voltage–time area (VTA), line-commutated converter-based high-voltage direct current (LCC-HVDC) system, nonlinear ac arc resistance.**

I. Introduction

COMMUTATION failures (CFs) caused by ac faults in line-commutated converter-based high-voltage direct current (LCC-HVDC) systems can cause temporary power transmission interruptions. It has been proven that an insufficient commutation voltage–time area (VTA) may cause a reduction in the extinction angle, thereby triggering CFs [1]. On this basis, extensive discussions have been conducted on the impacts of the ac system strength, direct current, inverter bus voltage drop and harmonic interaction on CFs [2], [3], [4], [5]. Among these factors, the voltage drop is particularly critical for CFs.

As a crucial factor affecting the commutation voltage, the fault resistance has mostly been treated as a constant in previous studies in this field. In fact, ac line faults are usually accompanied by arcs, which exhibit periodic high-resistance characteristics at each zero crossing of the fault current [6], [7], [8]. As illustrated in Fig. 1, the fault resistance in the inverter-side ac system comprises a nonlinear arc resistance R_{arc} and a transition resistance R_{con} [9]. Such periodic variation in the fault resistance will inevitably affect the commutation bus voltage, but due to the tendency of previous studies to focus on the fundamental wave characteristics after a fault and to assume a constant fault resistance, this phenomenon has not been sufficiently investigated. Notably, arc-induced periodic voltage distortions have been observed by high-frequency recorders in practical engineering projects [8]. Against this background, a transient calculation method for the commutation VTA is mathematically derived in this letter. Moreover, the impacts of arc-induced voltage distortions on CFs under various fault conditions are analyzed.

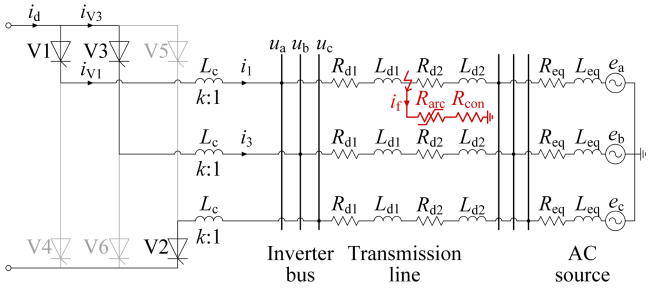

Fig. 1. Schematic of the commutation process from V1 to V3 under a single-line-to-ground fault.

II. Commutation Process Analysis

A. Commutation Voltages and VTAs Under Faults

Taking the commutation process shown in Fig. 1 as a study case, based on VTA theory, successful commutation from V1 to V3 requires that

$$\int_{\alpha}^{\pi-\gamma} (u_{\mathrm{a}} - u_{\mathrm{b}})\,\mathrm{d}\,(\omega t) = k\omega L_{\mathrm{c}}\,(i_{\mathrm{d0}} + i'_{\mathrm{d}}) \tag{1}$$

where t denotes the time, u_{a} and u_{b} are the commutation voltages, k denotes the transformer ratio, i_{d0} and i'_{d} are the dc currents at the beginning and end of the commutation process, i_{V1} and i_{V3} are the currents flowing through thyristors V1 and V3, respectively, L_{c} denotes the commutation inductance, α denotes the firing angle, γ denotes the extinction angle, and ω denotes the angular frequency.

The left-hand and right-hand sides of (1) are defined as the supplied VTA and the demanded VTA, respectively. For a commutation process, if the extinction angle γ, which is influenced by the dc current and commutation voltages, is less than the critical value γ_0, a CF occurs.

Manuscript received 24 January 2024; revised 22 February 2024; accepted 16 March 2024. Date of publication 20 March 2024; date of current version 4 September 2024. This work was supported by the National Natural Science Foundation of China under Grant 52277125. *(Corresponding author: Chenguang Yan.)*

The authors are with the State Key Laboratory of Electrical Insulation and Power Equipment, Xi'an Jiaotong University, Xi'an 710049, China (e-mail: chgyan@xjtu.edu.cn; yhx741088533@stu.xjtu.edu.cn; 281220011234@stu.xjtu.edu.cn; jshazp990528@stu.xjtu.edu.cn; bhzhang@xjtu.edu.cn).

Color versions of one or more figures in this article are available at https://doi.org/10.1109/TPEL.2024.3379520.

Digital Object Identifier 10.1109/TPEL.2024.3379520

For the single-line-to-ground fault shown in Fig. 1, the following equations are satisfied:

$$u_{\mathrm{a}} = R_{\mathrm{d1}} i_1 + L_{\mathrm{d1}} \frac{\mathrm{d}i_1}{\mathrm{d}t} + R_2 \left(i_1 - i_{\mathrm{f}}\right) + L_2 \frac{\mathrm{d}\left(i_1 - i_{\mathrm{f}}\right)}{\mathrm{d}t} + e_{\mathrm{a}} \quad (2)$$

$$u_{\mathrm{b}} = R_{\mathrm{d1}} i_3 + L_{\mathrm{d1}} \frac{\mathrm{d}i_3}{\mathrm{d}t} + R_2 i_3 + L_2 \frac{\mathrm{d}i_3}{\mathrm{d}t} + e_{\mathrm{b}} \quad (3)$$

where i_1 and i_3 are the primary-side currents of the converter transformers; i_{f} is the fault current; e_{a} and e_{b} are the source voltages; L_{d1} and R_{d1} are the transmission line inductance and resistance, respectively, from the fault point to the commutation bus; and L_2 and R_2 are the equivalent inductance and resistance from the fault point to the ac source

$$R_2 = R_{\mathrm{d2}} + R_{\mathrm{eq}} \quad (4)$$

$$L_2 = L_{\mathrm{d2}} + L_{\mathrm{eq}} \quad (5)$$

where L_{d2} and R_{d2} are the transmission line inductance and resistance, respectively, and L_{eq} and R_{eq} are the equivalent inductance and resistance of the ac source.

For the faulty branch, the relationship between the fault current i_{f} and the nonlinear arc resistance R_{arc} can be expressed by the experimentally verified Schwarz arc model, in which the arc cooling power and arc time constant are considered as power functions of arc resistance [10]

$$\frac{1}{R_{\mathrm{arc}}} \frac{\mathrm{d}R_{\mathrm{arc}}}{\mathrm{d}t} = \frac{R_{\mathrm{arc}}^m}{\tau} \left(1 - \frac{u_{\mathrm{arc}} i_{\mathrm{f}} R_{\mathrm{arc}}^n}{P}\right) \quad (6)$$

$$u_{\mathrm{arc}} = i_{\mathrm{f}} R_{\mathrm{arc}} \quad (7)$$

where u_{arc} denotes the arc voltage, P denotes the arc cooling power, τ denotes the arc time constant, the parameters m and n are arc constants, and R_{con} is the transition resistance.

Upon the substitution of (6) and (7) into (2), the expression for the commutation voltage during the commutation process becomes

$$u_{\mathrm{a}} = R_{\mathrm{ac}} i_1 + L_{\mathrm{ac}} \frac{\mathrm{d}i_1}{\mathrm{d}t} - u'_1 - u'_2 + e_{\mathrm{a}} \quad (8)$$

where

$$R_{\mathrm{ac}} = R_{\mathrm{d1}} + R_{\mathrm{d2}} + R_{\mathrm{eq}} \quad (9)$$

$$L_{\mathrm{ac}} = L_{\mathrm{d1}} + L_{\mathrm{d2}} + L_{\mathrm{eq}} \quad (10)$$

$$u'_1 = R_2 \sqrt{P R_{\mathrm{arc}}^{-1-n} - \tau P R_{\mathrm{arc}}^{-2-m-n} \frac{\mathrm{d}R_{\mathrm{arc}}}{\mathrm{d}t}} \quad (11)$$

$$u'_2 = L_2 P^{\frac{1}{2}} \times \frac{\left[(2+m+n)\tau R_{\mathrm{arc}}^{-1} \frac{\mathrm{d}R_{\mathrm{arc}}}{\mathrm{d}t} - (1+n) R_{\mathrm{arc}}^m\right] \frac{\mathrm{d}R_{\mathrm{arc}}}{\mathrm{d}t} - \tau \frac{\mathrm{d}^2 R_{\mathrm{arc}}}{\mathrm{d}t^2}}{2\sqrt{R_{\mathrm{arc}}^{3+2m+n} - \tau R_{\mathrm{arc}}^{2+m+n} \frac{\mathrm{d}R_{\mathrm{arc}}}{\mathrm{d}t}}}. \quad (12)$$

By substituting (3) and (8) into (1), the VTA equation during the single-line-to-ground fault is obtained

$$\int_{\alpha}^{\pi-\gamma} \left(u_{\mathrm{abN}} - u'_1 - u'_2\right) \mathrm{d}\left(\omega t\right) = k\omega L_c \left(i_{d0} + i'_d\right) \quad (13)$$

where u_{abN} can be calculated as

$$u_{\mathrm{abN}} = R_{\mathrm{ac}} \left(i_1 - i_3\right) + L_{\mathrm{ac}} \frac{\mathrm{d}\left(i_1 - i_3\right)}{\mathrm{d}t} + e_{\mathrm{a}} - e_{\mathrm{b}}. \quad (14)$$

The three-line diagram of another frequently occurring type of line fault, namely, a line-to-line fault, is depicted in Fig. 2. For this fault, the faulty phase commutation voltages are

$$u_{\mathrm{a}} = R_{\mathrm{d1}} i_1 + L_{\mathrm{d1}} \frac{\mathrm{d}i_1}{\mathrm{d}t} + R_2 \left(i_1 - i_{\mathrm{f}}\right) + L_2 \frac{\mathrm{d}\left(i_1 - i_{\mathrm{f}}\right)}{\mathrm{d}t} + e_{\mathrm{a}} \quad (15)$$

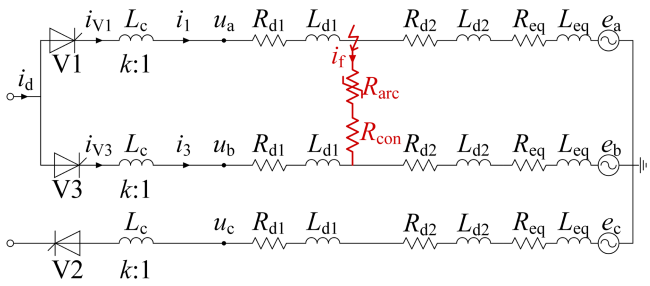

Fig. 2. Schematic of the commutation process from V1 to V3 under a line-to-line fault.

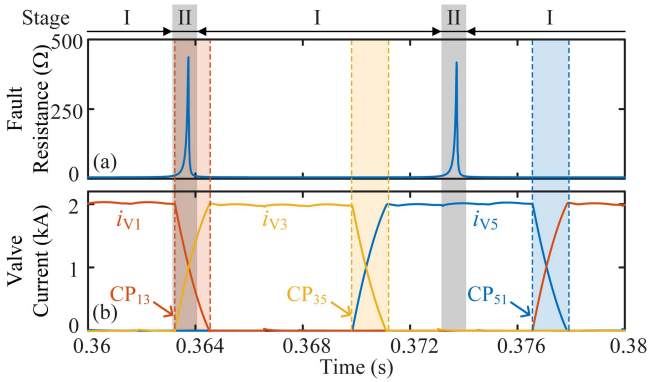

Fig. 3. Different commutation processes under an arc fault. (a) Fault resistance; (b) valve currents of thyristors V1, V3, and V5.

$$u_{\mathrm{b}} = R_{\mathrm{d1}} i_3 + L_{\mathrm{d1}} \frac{\mathrm{d}i_3}{\mathrm{d}t} + R_2 \left(i_3 + i_{\mathrm{f}}\right) + L_2 \frac{\mathrm{d}\left(i_3 + i_{\mathrm{f}}\right)}{\mathrm{d}t} + e_{\mathrm{b}}. \quad (16)$$

Upon the substitution of (6) and (7) into (15) and (16), the expressions for the commutation voltages during the commutation process become

$$u_{\mathrm{a}} = R_{\mathrm{ac}} i_1 + L_{\mathrm{ac}} \frac{\mathrm{d}i_1}{\mathrm{d}t} - u'_1 - u'_2 + e_{\mathrm{a}} \quad (17)$$

$$u_{\mathrm{b}} = R_{\mathrm{ac}} i_3 + L_{\mathrm{ac}} \frac{\mathrm{d}i_3}{\mathrm{d}t} + u'_1 + u'_2 + e_{\mathrm{b}}. \quad (18)$$

Similarly, the VTA equation under this line-to-line fault can be expressed as follows:

$$\int_{\alpha}^{\pi-\gamma} \left(u_{\mathrm{abN}} - 2u'_1 - 2u'_2\right) \mathrm{d}\left(\omega t\right) = k\omega L_c \left(i_{d0} + i'_d\right). \quad (19)$$

Since the commutation voltages are calculated based on the instantaneous values of the primary-side currents, source voltages and arc resistance, as seen from (8), (17), and (18), the theoretical derivation is not affected by the winding connection of the converter transformers.

B. *Effects of Nonlinear Arc Resistance*

As seen from (13) and (19), for both single-line-to-ground faults and line-to-line faults, the supplied VTA is affected by the arc cooling power P and the arc resistance R_{arc}. In this letter, the parameters are set to $\tau = 60\,\mu$s, $m = 0.06$, and $n = 1$ [10]. As shown in Fig. 3, the fault arc exhibits nonlinear resistance characteristics with intermittent high resistance. This is caused by the arc zero-off effect in stage II, which results in high resistance, in combination with the relatively low resistance in stage I.

For commutation processes that occur during stage I, such as CP_{35} and CP_{51}, the arc resistance behaves as a steady-state arc resistance

throughout. However, for commutation processes such as CP_{13}, due to the overlap between the commutation process and stage II, the arc resistance experiences a steep change. These phenomena lead to different effects of the nonlinear arc resistance on the supplied VTA.

1) Commutation Processes During Stage I: During stage I, the arc resistance remains relatively low. Since the change rate of the arc resistance is small, the derivative terms in (11) and (12) can be neglected

$$u'_1 \approx \frac{R_2}{R_{\text{arc}}}\sqrt{P} \tag{20}$$

$$u'_2 \approx 0. \tag{21}$$

Therefore, the supplied VTA for a commutation process in stage I is determined only by the arc cooling power P, which is related to the fault current and transition resistance. Consequently, the nonlinear arc resistance has little impact on the supplied VTAs for the commutation processes during stage I.

$$\text{VTA}_{\text{sup}} \approx \int_{\alpha}^{\pi-\gamma}\left(u_{\text{abN}} - \frac{R_2}{R_{\text{arc}}}\sqrt{P}\right)\text{d}(\omega t) \tag{22}$$

2) Commutation Processes During Stage II: For a commutation process near the zero-crossing point of the arc current, the arc resistance will experience a substantial transient variation. Under these conditions, the fault-induced commutation voltage fluctuations can be derived from (6), (11), and (12) as follows:

$$u'_1 \approx 0 \tag{23}$$

$$u'_2 = L_2 P\left(\text{A}i_{\text{f}}^{-1} + \text{B}i_{\text{f}} + \text{C}i_{\text{f}}^{3}\right) \tag{24}$$

where

$$\text{A} = \frac{0.53}{\tau R_{\text{arc}}^{1.94}} - \frac{\tau}{2R_{\text{arc}}^{3.06}}\frac{\text{d}^2 R_{\text{arc}}}{\text{d}t^2} \tag{25}$$

$$\text{B} = -\frac{2.06R_{\text{arc}}^{0.06}}{\tau P} \tag{26}$$

$$\text{C} = \frac{1.53R_{\text{arc}}^{2.06}}{\tau P^2}. \tag{27}$$

In (24), since the arc current is near zero, the variation in u'_2 is mainly determined by the inverse term of the current. For $\tau = 60\ \mu$s, the coefficient A mainly depends on the first part and decreases with the increase of arc resistance. Therefore, as seen by combining (23) and (24) with (13) or (19), the effect of the nonlinear arc resistance is determined by the fault current.

$$\text{VTA}_{\text{sup}} \approx \int_{\alpha}^{\pi-\gamma}\left[u_{\text{abN}} - L_2 P\left(\text{A}i_{\text{f}}^{-1} + \text{B}i_{\text{f}} + \text{C}i_{\text{f}}^{3}\right)\right]\text{d}(\omega t) \tag{28}$$

It is obvious that if the fault current is positive, the nonlinear arc resistance causes an increase in VTA_{sup}, whereas it causes VTA_{sup} to decrease if the fault current is negative.

III. Case Study

In this letter, the CIGRE HVDC benchmark model was implemented in RSCAD to evaluate the impact of the nonlinear arc resistance [11]. A transmission line consisting of LGJ-500 conductors with a length of 50 km was adopted in the inverter-side ac system. For each step, the nonlinear arc resistance R_{arc} calculated by means of the Runge–Kutta method served as an input parameter for the real-time digital simulator (RTDS) platform shown in Fig. 4.

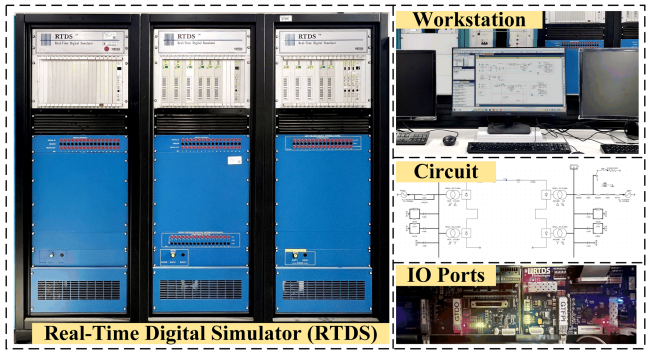

Fig. 4. RTDS setup for the studied system.

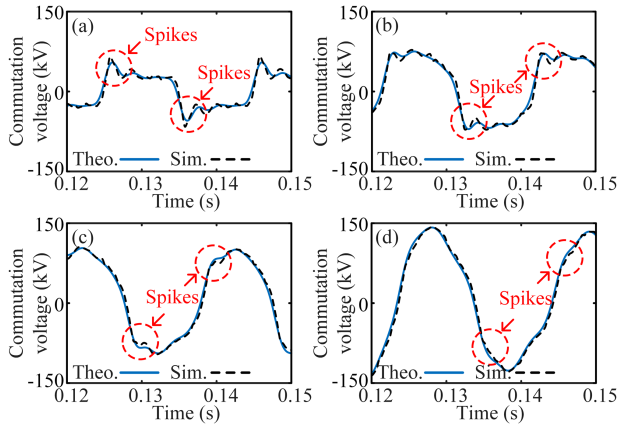

Fig. 5. Faulty-phase commutation voltages under single-line-to-ground faults with different transition resistances. (a) $R_{\text{con}} = 0\ \Omega$; (b) $R_{\text{con}} = 5\ \Omega$; (c) $R_{\text{con}} = 10\ \Omega$; (d) $R_{\text{con}} = 20\ \Omega$.

A. Single-Line-to-Ground Faults

The faulty-phase commutation voltages under A-phase single-line-to-ground faults at a location 10% of the transmission line away from the commutation bus with different transition resistances are shown in Fig. 5. The blue solid lines and the black dashed lines represent the theoretical values calculated from (8) and the simulated values from RTDS, respectively. Both the simulated and theoretical results show that the nonlinear arc resistance acts as a source of voltage distortions, generating harmonics in the commutation bus voltage. As illustrated in Fig. 5(a)–(c), these voltage harmonics mainly manifest as periodic spikes during stage II. Moreover, the commutation voltage distortions caused by the fault arc increase as the transition resistance decreases.

Based on VTA theory, these arc-induced spikes in the faulty-phase voltage may affect the commutation process. Taking an A-phase-to-ground fault as a study case, these spike-shaped voltage distortions during commutation processes CP_{24} and CP_{51} can lead to a decrease in the commutation VTA and even directly advance the zero-crossing points, as shown in Fig. 6. However, when these spikes appear during commutation processes CP_{13} and CP_{46}, they instead result in an increase in the commutation VTA, as shown in Fig. 7. In Figs. 6 and 7, the solid blue and orange lines represent the commutation voltages under the A-phase-to-ground fault, and the dashed lines represent the commutation voltages when the arc is simplified as a fixed resistance.

To further probe the impact of the nonlinear arc resistance on the commutation process, faults occurring at different locations with no transition resistances are simulated. Comparisons of the VTAs for faults occurring at different locations away from the commutation

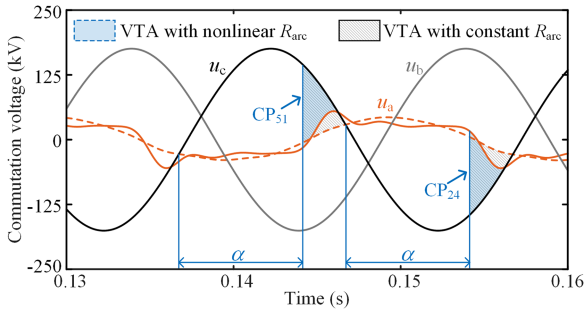

Fig. 6. Schematic illustration of arc-induced spikes that decrease the VTA.

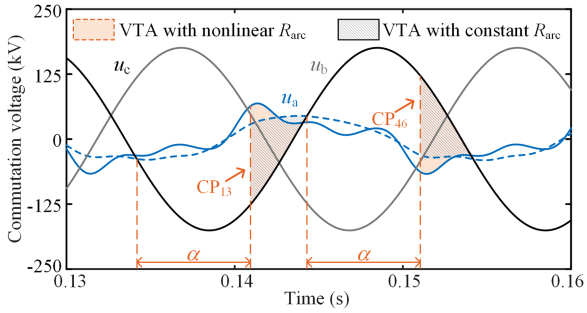

Fig. 7. Schematic illustration of arc-induced spikes that increase the VTA.

TABLE I
VTAs FOR FAULTS OCCURRING AT DIFFERENT LOCATIONS

d	VTA for CP_{13} or CP_{46} (kV·ms)		VTA for CP_{24} or CP_{51} (kV·ms)	
	Nonlinear R_{arc}	Simplified R_{arc}	Nonlinear R_{arc}	Simplified R_{arc}
0%	200.9	167.9	188.6	199.6
20%	203.6	171.8	189.5	208.7
40%	207.6	180.1	205.0	224.9
60%	209.3	195.5	208.2	235.3
80%	202.7	196.3	229.6	241.3
100%	202.8	206.7	234.8	241.4

bus are presented in Table I. To obtain the maximum possible VTA, the corresponding firing angle was set to 90°, which is the minimum value from the inverter-side control system. When the fault occurs at $d = 0\%$, the increase in VTA_{ba} reaches its maximum value of 33.0 kV·ms. At $d = 60\%$, the maximum decrease in VTA_{ac} of 27.1 kV·ms occurs, causing a reduction in the extinction angle and hindering the commutation process. Notably, for single-line-to-ground faults, these voltage distortions decrease the VTA supported by u_a and u_c, whereas they increase the VTA supported by u_a and u_b.

B. Line-to-Line Faults

The commutation line voltages u_{ab} and faulty phase voltages u_a and u_b for line-to-line faults at a location 10% of the transmission line away from the commutation bus with different transition resistances are shown in Figs. 8 and 9. In Fig. 8, the blue solid lines and the black dashed lines represent the theoretical values calculated from (17) and (18) and the simulated values from RTDS, respectively. In Fig. 9, the red solid lines and brown dashed lines represent the theoretical and simulated values of u_a, respectively, and the blue solid lines and black dashed lines represent the theoretical and simulated values of u_b, respectively. Similarly, the distortions from the nonlinear arc resistance are larger for faults with lower transition resistances. Moreover, due to

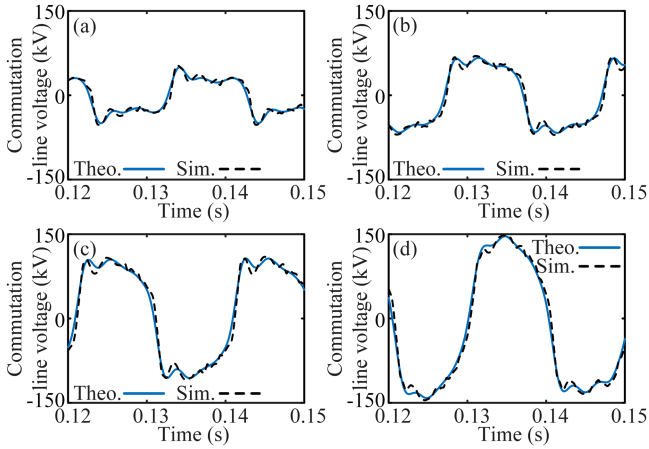

Fig. 8. Commutation line voltages u_{ab} under line-to-line faults with different transition resistances. (a) $R_{con} = 0\ \Omega$; (b) $R_{con} = 5\ \Omega$; (c) $R_{con} = 10\ \Omega$; (d) $R_{con} = 20\ \Omega$.

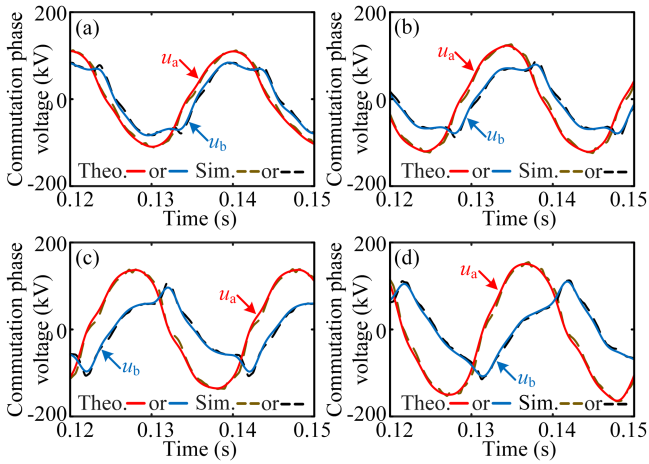

Fig. 9. Commutation phase voltages u_a and u_b under line-to-line faults with different transition resistances. (a) $R_{con} = 0\ \Omega$; (b) $R_{con} = 5\ \Omega$; (c) $R_{con} = 10\ \Omega$; (d) $R_{con} = 20\ \Omega$.

TABLE II
VTAs FOR FAULTS OCCURRING AT DIFFERENT LOCATIONS

d	VTA for CP_{13} or CP_{46} (kV·ms)		VTA for CP_{24} or CP_{51} (kV·ms)	
	Nonlinear R_{arc}	Simplified R_{arc}	Nonlinear R_{arc}	Simplified R_{arc}
0%	94.4	41.0	293.0	290.5
20%	88.1	39.1	288.7	288.3
40%	85.0	39.1	287.6	286.5
60%	66.8	38.3	284.9	286.1
80%	46.0	38.9	285.1	285.5
100%	45.4	38.2	282.9	286.3

the failure of commutation processes CP_{13} and CP_{46}, the distortion in u_b is larger than that in u_a. In Fig. 9, as R_{con} increases, because of the decreasing voltage offset caused by the line-to-line fault current, the phase difference between u_a and u_b shows an increasing trend.

Table II presents comparisons of the VTAs for faults occurring at different locations. In contrast to single-line-to-ground faults, the voltage distortions from nonlinear arc resistance mainly increase the VTA supported by the fault line voltage and has little impact on other commutation processes.

IV. Conclusion

Previous studies investigating CFs have simplified the nonlinearity of the fault arc resistance during line faults and thus have neglected the influence of the arc zero-off effect on the commutation process. This letter presents the first analysis of the impact of a nonlinear fault arc resistance on the commutation VTA under different fault conditions. With the fault arc acting as a source of voltage distortions, spike-shaped voltage distortions appear in the faulty-phase voltages. Both theoretical analyses and RTDS-based simulation results confirm that these voltage distortions reduce the $\mathrm{VTA_{ac}}$ and advance the commutation voltage crossing point but increase the $\mathrm{VTA_{ab}}$ in the case of A-phase-to-ground faults. However, these distortions increase the VTA in the case of line-to-line faults. These findings reveal a significant fault transient characteristic that impacts CFs, providing insight into the further improvement of CF suppression strategies.

References

[1] C. Guo, Y. Liu, C. Zhao, X. Wei, and W. Xu, "Power component fault detection method and improved current order limiter control for commutation failure mitigation in HVDC," *IEEE Trans. Power Del.*, vol. 30, no. 3, pp. 1585–1593, Jun. 2015.

[2] H. Xiao, X. Duan, Y. Zhang, T. Lan, and Y. Li, "Analytically quantifying the impact of strength on commutation failure in hybrid multi-infeed HVDC systems," *IEEE Trans. Power Electron.*, vol. 37, no. 5, pp. 4962–4967, May 2022.

[3] J. Ouyang, M. Pang, Z. Zhang, and J. Yu, "Fault security region modeling and adaptive current control method for the inverter station of DC transmission system," *IEEE Trans. Power Del.*, vol. 37, no. 6, pp. 4979–4988, Dec. 2022.

[4] S. Mirsaeidi, X. Dong, D. Tzelepis, D. M. Said, A. Dyśko, and C. Booth, "A predictive control strategy for mitigation of commutation failure in LCC-based HVDC systems," *IEEE Trans. Power Electron.*, vol. 34, no. 1, pp. 160–172, Jan. 2019.

[5] L. Wang, W. Yao, Y. Xiong, Z. Shi, and J. Wen, "Commutation failure analysis and prevention of UHVDC system with hierarchical connection considering voltage harmonics," *IEEE Trans. Power Del.*, vol. 37, no. 4, pp. 3142–3154, Aug. 2022.

[6] M. Ghazizadeh-Ahsaee, "Accurate arcing fault location method for M-terminal transmission lines," *Int. J. Elect. Power Energy Syst.*, vol. 98, pp. 147–155, Jun. 2018.

[7] A. Marroquin, A. Rehman, and A. Madani, "High-voltage arc flash assessment and applications," *IEEE Trans. Ind. Appl.*, vol. 56, no. 3, pp. 2205–2215, May/Jun. 2020.

[8] B. Wang, X. Wei, and Y. Xia, "An innovative arc fault model and detection method for circuit breakers in LCC-HVDC AC filter banks," *IEEE Trans. Power Del.*, vol. 38, no. 6, pp. 3888–3899, Dec. 2023.

[9] M. Wei, W. Liu, F. Shi, H. Zhang, Z. Jin, and W. Chen, "Distortion-controllable arc modeling for high impedance arc fault in the distribution network," *IEEE Trans. Power Del.*, vol. 36, no. 1, pp. 52–63, Feb. 2021.

[10] H. Wu, L. Yuan, L. Sun, and X. Li, "Modeling of current-limiting circuit breakers for the calculation of short-circuit current," *IEEE Trans. Power Del.*, vol. 30, no. 2, pp. 652–656, Apr. 2015.

[11] M. O. Faruque, Y. Zhang, and V. Dinavahi, "Detailed modeling of CIGRE HVDC benchmark system using PSCAD/EMTDC and PSB/SIMULINK," *IEEE Trans. Power Del.*, vol. 21, no. 1, pp. 378–387, Jan. 2006.